High-latitude electrodynamics specified in SAMI3 using AMPERE field-aligned currents

A.T. Chartier[1], J.D. Huba[2], D.S. Sitaram[1], V.G. Merkin[1], B.J. Anderson[1], S.K. Vines[1]

[1] Johns Hopkins University/Applied Physics Laboratory, Laurel, MD 20723

[2] Syntek Technologies, Fairfax, VA 22031

Abstract

A new technique has been developed in which the high-latitude electric potential is determined from field-aligned current observations from the Active Magnetosphere and Planetary Electrodynamics Response Experiment (AMPERE) and conductances modeled by Sami3 is Also a Model of the Ionosphere (SAMI3). This is a development of the Magnetosphere-Ionosphere Coupling (MIX) approach first demonstrated by Merkin and Lyon (2010). An advantage of using SAMI3 is that the model can be used to predict Total Electron Content (TEC) in the polar caps, based on the AMPERE-derived potential solutions. 23 May 2014 is chosen as a case study to assess the new technique for a moderately disturbed case (min Dst: -36 nT, max AE: 909 nT) with good GPS data coverage. The new AMPERE/SAMI3 solutions are compared against independent GPS-based TEC observations from the Multi-Instrument Data Analysis Software (MIDAS) by Mitchell and Spencer, 2003, and against Defense Meteorological Satellite Program (DMSP) ion drift data. The comparison shows excellent agreement between the location of the tongue of ionization in the MIDAS GPS data and the AMPERE/SAMI3 potential pattern, and good overall agreement with DMSP drifts. SAMI3 predictions of high-latitude TEC are much improved when using the AMPERE-derived potential as compared to that of the Weimer (2005) model. The two potential models have substantial differences, with Weimer producing an average 77 kV cross-cap potential versus 60 kV for the AMPERE-derived potential. The results indicate that the 66-satellite Iridium constellation provides sufficient resolution of field-aligned currents to estimate large-scale ionospheric convection as it impacts TEC.

Plain language summary

Plasma in the ionosphere convects across high latitudes in response to electric fields generated by solar wind driving of Earth's magnetosphere. Magnetic data from the 66-satellite Iridium satellite constellation is routinely analyzed to measure the electric currents flowing between the ionosphere and magnetosphere. In this paper, we combined these observed field-aligned currents with a model of the ionospheric conductance to estimate the corresponding electric field in the ionosphere. We used these electric field estimates to specify the plasma convection in a first-principles ionosphere model, and compared the results against independent data in a moderately disturbed period. The results of our case study indicate that the technique works well, although plasma convection is not the only factor that causes uncertainty into predictions of the high-latitude

ionosphere. The data used here can be made available in near-real-time, so it is possible that our technique could be adopted for operational space weather prediction.

Key points

AMPERE field-aligned currents have been combined with the SAMI3 model to estimate the high-latitude potential

Independent validation of the new technique using satellite drifts and ground-based TEC indicates good agreement overall

The SAMI3 model performs better in this case when using AMPERE-derived potentials than when using the empirical Weimer potential

1. Introduction

Over the past several decades, great progress has been made in specifying the ionosphere through first-principles modeling and data assimilation. Ionospheric specification at high latitudes remains challenging because of the influence of the solar wind and magnetosphere on the ionosphere, especially in terms of plasma convection (e.g. Spencer and Mitchell, 2007; Bust et al., 2007; Chartier et al., 2019), as well as the relatively poor data coverage compared to other regions. The northern high latitudes are becoming increasingly relevant in terms of space weather due to the opening of the Arctic to shipping and mineral exploration. This is reflected in a focus on the region from several U.S. government agencies, notably the Department of the Air Force in its Arctic Strategy (Barrett et al., 2020) and the National Science Foundation's Big Idea: Navigating the New Arctic. The lack of ground networks in this area results in increased reliance on wireless signals, which are susceptible to ionospheric disturbances.

Data from the Active Magnetosphere and Planetary Electrodynamics Response Experiment (AMPERE, Anderson et al., 2000; 2002, Waters et al., 2001; 2020) provide the most reliable and ubiquitous means of specifying high-latitude ionospheric electrodynamics, with field-aligned current measurements available from over 70 satellites in six polar low-Earth orbits, yielding global measurement coverage at all latitudes every 10 minutes. The AMPERE dataset allows for the resolution of the full Region 1 and Region 2 current system in near real time and across both northern and southern polar caps (e.g. Anderson et al., 2008). Understandably, this dataset has featured prominently in many recent efforts to specify the high-latitude electrodynamics, such as Assimilative Mapping of Ionospheric Electrodynamics (Cousins et al., 2015) and Assimilative Mapping of Geospace Observations (Matsuo et al., 2019).

To determine the high-latitude potential from the field-aligned current distribution, it is necessary to know the ionospheric perpendicular conductances (Pedersen and Hall). The most important determining factors of the conductances are the solar EUV flux, the average energy and energy flux of energetic particles and the neutral upper atmospheric density and composition. Several approaches

exist to address this problem. The simplest is the assumption of constant conductance (used by Merkin and Lyon, 2010), while others use empirical relations and modeling to estimate conductance from other parameters (e.g. Robinson and Vondrak, 1984; Robinson et al., 1987; Zhang et al., 2015; McGranaghan et al., 2016). First-principles models of the ionosphere/upper atmosphere (e.g. Quegan et al., 1982; Roble et al., 1988; Huba et al., 2000; 2008) also contain all the parameters needed to calculate the conductance (altitudinal profiles of electron density and neutral atmospheric density).

A major obstacle to the development of reliable high-latitude electrodynamic solutions has been the challenge of validation. The high-latitude electric potential is not directly observable, and even its derivative, the high-latitude electric field, is observed only through its effect on ions via the **E**x**B** drift. As a result of this lack of direct comparison data, many recent developments in **E**x**B** drift solutions have been published without validation (e.g. Bristow et al., 2016; Gjerloev et al., 2018). In order to validate convection maps, some authors have used ionospheric F-region electron density structures as a tracer of the ExB drift. Wang et al. (2018) and Ramirez et al. (2019) have used the observed motion of high-latitude electron density structures to assess the accuracy of Weimer's (2005) empirical model and Ruohoniemi and Baker's (1998) SuperDARN-driven high-latitude potentials.

2. Method

In this investigation, we aim to specify the high-latitude electrodynamics in order to predict the generation and development of ionospheric electron density structures (e.g. the tongue of ionization, polar cap patches). We then test our predictions against independent GPS-based TEC data showing those structures, and against satellite ion drift data. The approach is as follows:

a) determine the Pedersen (Σ_P) and Hall (Σ_H) conductances from SAMI3,

b) calculate the high-latitude potential (Ψ) using Σ_P, Σ_H and AMPERE-observed field-aligned currents ($\boldsymbol{J}$),

c) use Ψ to calculate **E**x**B** plasma drifts in SAMI3

d) compare simulation results to data

The potential is calculated at a 10-minute cadence, matching the latitude resampling cadence of the Iridium satellites used for AMPERE. The outputs are the full set of electrodynamic parameters (Σ_P, Σ_H, $\Sigma_{||}$, Ψ, $\boldsymbol{J}$) as well as the ionospheric electron density distribution, which can be vertically integrated to produce Total Electron Content (TEC). The electric potentials are compared against Defense Meteorological Satellite Program (DMSP) horizontal ion drift data (e.g. Hairston and Heelis, 1993) during the period of interest. The TEC output is compared against images from the University of Bath's Multi-Instrument Data Analysis Software (Mitchell and Spencer, 2003; Spencer and Mitchell, 2007), which uses ground-based GPS data. The MIDAS algorithm's

ability to image the tongue of ionization and patches has previously been validated by Wang et al., 2018, Spencer and Mitchell, 2007, and others.

For this demonstration, we have applied the technique to a magnetically active period in the most recent solar maximum: 21-25 May 2014. This period contains relatively strong field-aligned currents, both because of the elevated magnetic activity and because the northern polar cap is in sunlight. Figure 1 shows the IMF Bz component and the Kyoto Disturbance Storm Time (Dst) and Auroral Electrojet (AE) indices for this period. On 23 May 2014, Bz reached a minimum of -7.5 nT at 19 UT, Dst reached a minimum of -36 nT at 21 UT, while the maximum AE of 909 nT occurred earlier, at 17 UT. The case could be summarized as a weak geomagnetic storm with substantial substorm activity.

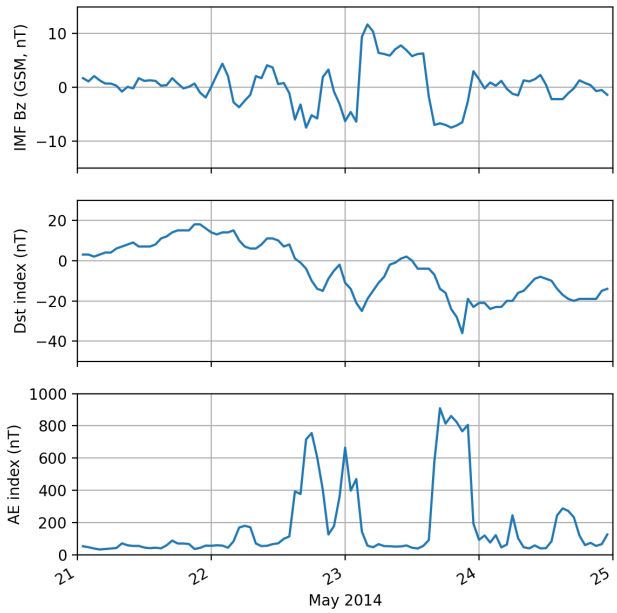

2.1 Conductances

Pedersen and Hall conductances are calculated from the SAMI3 model (*Huba et al.,* 2000; *Huba et al.,* 2008) following the standard relations described e.g. in Maeda (1977). We have not included nonlinear or turbulent sources of Pedersen conductance such as those described by Merkin et al., 2005; Dimant and Oppenheim, 2011 and Wiltberger et al., 2017. SAMI3 solves for the dynamic

plasma and chemical evolution of seven ion species (H^+, He^+, $N_2{}^+$, O^+, N^+, NO^+, and $O_2{}^+$) on a field-aligned magnetic apex coordinate grid (*Richmond*, 1995) extending up to 88° MLAT. Photoionization is calculated using solar flux from the EUV flux model for aeronomic calculations (EUVAC) by Richards et al. (1994). The Hardy model [*Hardy et al.*, 1985, 1989] provides auroral electron and ion precipitation estimates based on the K_P index. The neutral atmosphere is specified by the Horizontal Wind Model 2014 by *Drob et al.* [2015] and the Naval Research Laboratory's Mass Spectrometer Incoherent Scatter Model 2000 of neutral atmospheric densities by *Picone et al.* [2002]. An example of these conductances at 0 UT is shown in Figure 2. In this case, noon is at 0° longitude and therefore is on the right-hand side of the panels.

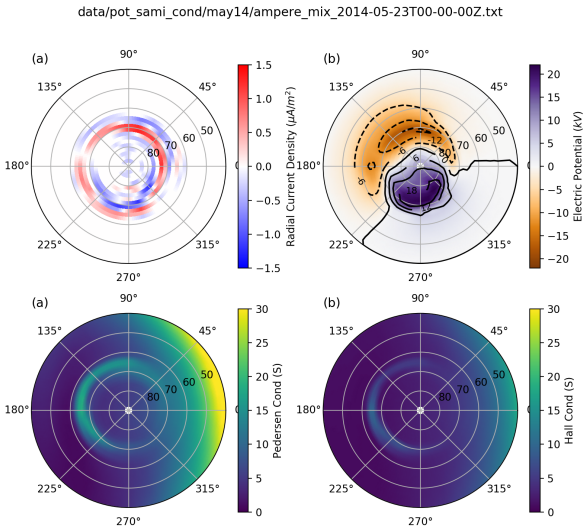

2.2 High-latitude potential

We use a Python version of REMIX, which is the electrostatic potential solver in the Grid Agnostic MHD with Extended Research Applications (GAMERA) global magnetosphere model (Sorathia et al., 2020). REMIX is a redeveloped version of the Magnetosphere-Ionosphere Coupler-Solver (MIX) developed originally by Merkin and Lyon (2010). In the application presented here, we solve for the high-latitude potential using field-aligned currents from AMPERE (Anderson et al., 2000, 2014, 2021) and the SAMI3 conductances described above. The underlying solution is based on the current continuity equation presented by *Wolf* (1983) and *Goodman* (1995), which is analogous to Ohm's Law. This is shown in Equation 1 (note that δ is the magnetic dip angle).

$$\nabla_\perp \bullet \begin{bmatrix} \Sigma_P \cos^{-2}\delta & \Sigma_H \cos^{-1}\delta \\ \Sigma_H \cos^{-1}\delta & \Sigma_P \end{bmatrix} \bullet \nabla_\perp \psi = \; j_{||}\cos \quad (1)$$

The solver operates in Solar Magnetic (SM) coordinates with the pole boundary based on the regularity constraint (Lewis & Bellan, 1991; Merkin & Lyon, 2010) and the lower latitude boundary condition setting Ψ=0 at 40^o MLAT.

Figure 3 shows an example REMIX potential solution (right) calculated from AMPERE field-aligned currents (left) and the SAMI3 conductances from Figure 2. The solver produces the expected two-cell convection pattern directly from the observed currents and modeled conductances, without relying on a background potential model.

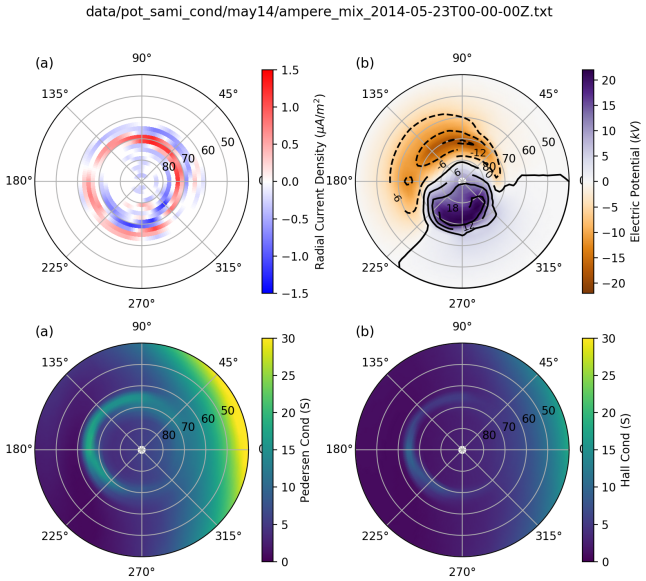

2.3 ExB drifts

The magnetospheric potential is mapped onto SAMI3's magnetic apex coordinates and superposed with the internal wind-driven dynamo. The spatial derivative of this combined potential is calculated to find the electric field **E**. The electric field produces **ExB** ion drifts in the model, resulting in predictions of largely photo-ionized F-region plasma flowing into the polar cap from the dayside.

3. Results

Over the course of the experiment, the most intense period of disturbances occurred in the later hours of 23 May 2014, between 19 – 22 UT. Relevant DMSP passes during this period were identified and used to assess the accuracy of the AMPERE-derived potentials. The flagged "good" data from UT Dallas were decimated and mapped to a geographic reference frame before plotting.

Results of three passes (two from F16 and one from F18, spaced by ~2 hours total) are shown in Figure 4, with the pass times indicated in each subplot. Note that these (and subsequent) plots are in geographic coordinates and so the subsolar point is in the bottom-left. The potentials closest to the center of each pass are shown. In these cases there was no great variation between timesteps across each pass, and the three cases are broadly consistent with each other. In all cases, DMSP velocities and AMPERE-derived potentials show close agreement in the evening cell (negative potential), where the velocity turning points match the location of the minimum potential, and the velocities line up well to the potential contours. However there are some discrepancies in the morning cell (shown in blue), where the DMSP data do not show the turning points that would be expected from the modeled potential.

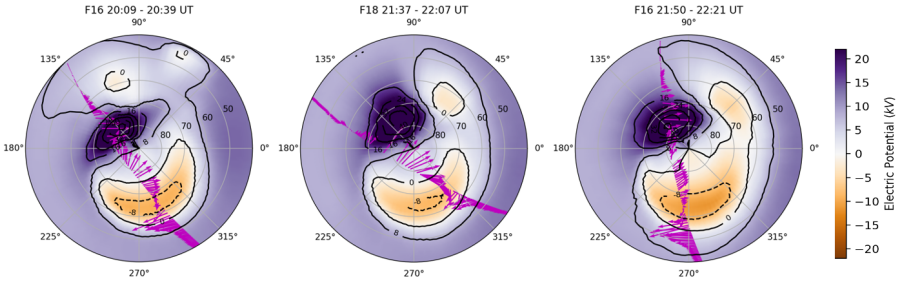

In Figure 5, the AMPERE-derived potentials from 19-22 UT are overlaid on TEC data from the MIDAS GPS-based tomographic imaging algorithm. The results indicate that our derived potential patterns are consistent with the independent TEC data. The tongue of ionization emanating from the US sector propagates directly along the path predicted by the potential contours (ion drifts are oriented along the contour lines, pointing from day to night in the center of the pattern). At other times (not shown), when Kp was lower, the potential is far smaller in magnitude and no such tongues of ionization are seen. The level of agreement between these two independent observational sets is remarkable, with azimuthal deviations in the tongue of ionization matched by variations in the dayside potential (e.g. at 22 UT).

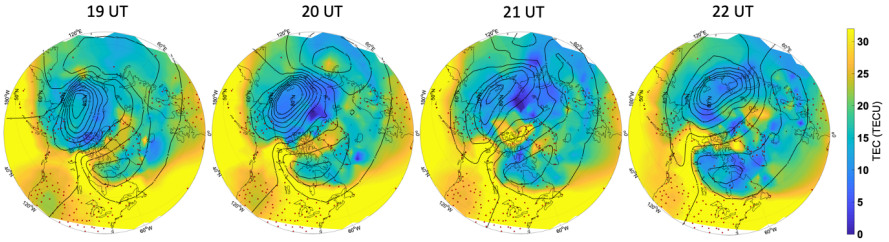

Given that the AMPERE-derived potential appears consistent with the TEC data, it is worth considering how the SAMI3 model's predictions of TEC compare to the data in the high-latitude region when using this potential. To assess the impact of this potential model, a SAMI3 run using the Weimer (2005) potential model is also included. This comparison is shown in Figure 6.

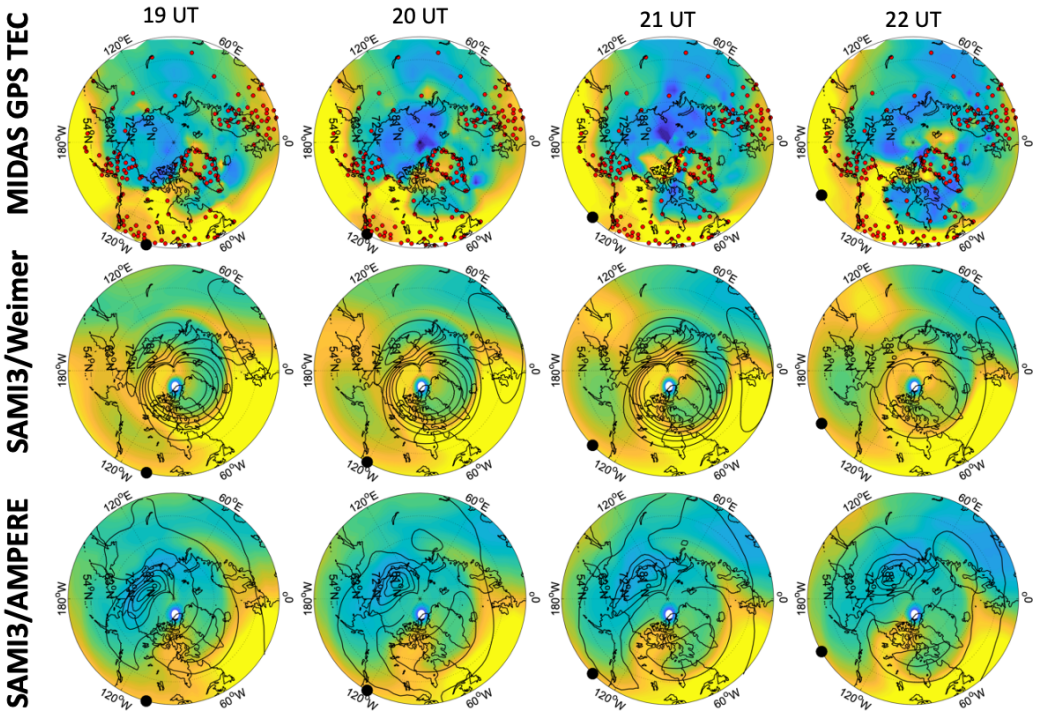

The comparison shows that the SAMI3 model more accurately reproduces the MIDAS GPS TEC data when using the AMPERE-derived potential. The location and extent of the tongue of ionization is more accurately modeled by SAMI3/AMPERE than by SAMI3/Weimer. Some common biases are present in both model runs, especially at lower latitudes (45 – 60° N). TEC is overestimated in the evening sector (0-90° W) and underestimated in the morning sector (150° E – 90° W). Although these biases are unrelated to the high-latitude potential, they play a role in skewing the formation of the tongue of ionization towards the evening sector in both model runs.

For most of this event, the Weimer potential is much larger than the AMPERE-derived potential. On average, the Weimer cross-cap potential is 77 kV whereas the AMPERE-derived potential is only 60 kV. This large potential causes an over-extension of the tongue of ionization in SAMI3/Weimer as compared to the GPS-derived TEC data. Figure 7 shows the extent of the two cross-cap potential options over the 23 May 2014 case (the plot shows the maximum and minimum values of the polar cap potential estimated by each technique).

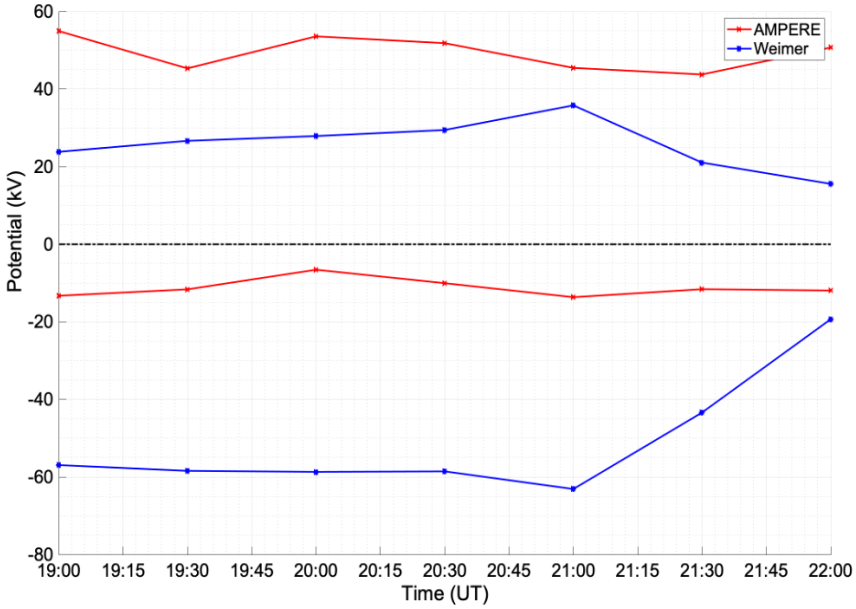

The Weimer potential has a negative bias averaging -13 kV, while the AMPERE-derived potential has a positive bias averaging 19 kV. This is reflected in the large evening cell of Weimer, whereas the AMPERE potential has a more pronounced morning cell.

4. Discussion

The high-latitude electric potential has been determined from AMPERE field-aligned currents and conductances modeled by SAMI3. This is a development of the MIX approach first demonstrated by Merkin and Lyon, 2010. An outcome of the use of SAMI3 in solving for the potential is that the model can be used to predict TEC in the polar caps, based on those potential solutions. This allows for independent validation of the technique against GPS-derived images of TEC from the MIDAS algorithm (Mitchell and Spencer, 2003; Spencer and Mitchell, 2007). Applied to the case of 23 May 2014, a period of moderate geomagnetic disturbance (K_P reached 5^+ between 21-24 UT), the AMPERE-derived potential results in high-latitude TEC predictions that are much closer to the observations than SAMI3 run with the Weimer (2005) model. Important biases remain in both versions of the model, especially at lower latitudes (45 – 60° N) where TEC is overestimated in the evening sector and underestimated in the morning sector. This skews the location of the tongue of ionization to later local times in both versions of the model. Comparison of the derived potentials against DMSP velocity data indicate good agreement in the evening cell, but some discrepancies in the morning cell. The bulk of F-region plasma is typically found post-noon, so the effects of this discrepancy should be limited in terms of formation of tongues of ionization and patches. The problem might be caused by low conductances in the morning cell, which would be expected to reduce the magnitude of field-aligned currents observed by AMPERE, or by low ion densities at DMSP altitudes affecting the performance of the drift meter.

The new AMPERE-derived potential and its relatively good performance in predicting high-latitude TEC serves as an indication of the large degree of uncertainty in high-latitude potential models. The Weimer potential is substantially larger than the AMPERE-derived potential (77 kV vs 60 kV) and is skewed towards the evening cell at -13 kV versus a +19 kV skew towards the morning cell in AMPERE. The two potentials also show a variety of smaller scale differences in terms of latitudinal extent and the shape of the dayside cusp. The comparison between the AMPERE-derived potential and the observed TEC data in Figure 5 shows a close match between the shape of the potential around the dayside cusp and the path of the tongue of ionization. This indicates that AMPERE's underlying dataset (the Iridium constellation of 66 operational satellites reporting magnetic perturbations every 10 minutes) has sufficient spatio-temporal resolution to capture the major features of polar cap plasma convection at scales of 100s of km and larger.

The conductance model represents a major source of uncertainty in the estimation of electric potentials from FAC observations. During testing, we assessed several conductance options, including constant conductances, solar EUV parameterization and the empirical model of Robinson et al. (2020), and found that none of them produced an improvement over the internal SAMI3/Hardy

conductance. Likewise the turbulent Pedersen conductance term of Dimant and Oppenheim (2011), whose effect is to reduce the strength of the electric potential, was not found to improve agreement with independent data in this case. In fact the AMPERE-derived potential was weaker than the Weimer potential even without consideration of the turbulent conductance term. It may be that competing biases caused this outcome. Future efforts towards accurate, global characterization of the ionospheric conductance will be useful in the application of this technique.

The high-latitude potential is of major importance to high-latitude ionospheric dynamics, but is not the only source of uncertainty in modeling the plasma distribution there. Other important factors include the reservoir of photo-ionized plasma on the subauroral dayside, and the plasma lifetimes in the polar cap (e.g. Chartier et al., 2019). Various SAMI3 driver options were tested with the aim of matching observed subauroral TEC levels (results not shown in this paper). These included the Flare Irradiance Spectral Model by Chamberlin et al. (2007) and the neutral atmosphere of the Thermosphere-Ionosphere-Mesosphere-Electrodynamics General Circulation Model by Roble and Ridley (1994). General conclusions about those models should not be drawn from this analysis but, in this case study, none of those options was able to match the observed levels of TEC as well as the configuration shown here. Future operational systems would benefit from ionospheric density assimilation schemes to better specify the sub-auroral plasma that feeds into the polar caps.

Conclusions

A case study of 23 May 2014 (a day with moderate geomagnetic activity) demonstrates the potential for integrating high-latitude electric potential estimates based on AMPERE observations into SAMI3. The new technique is useful in predicting high-latitude TEC. The AMPERE-derived potential is in good agreement with DMSP ion drifts overall, and closely matches the tongue of ionization observed in MIDAS GPS-derived TEC images of the northern polar cap. In this case, SAMI3's predictions of high-latitude TEC are much closer to the data when using AMPERE-derived potentials than when using the Weimer potential. The Weimer cross-polar cap potential is substantially larger than the AMPERE potential at 77 kV versus 60 kV. At least in this case, this investigation demonstrates that the AMPERE data has sufficient spatio-temporal resolution to predict TEC variations at scales of 100s of km and above.

Acknowledgements

The authors acknowledge support of National Science Foundation (NSF) CEDAR grant #1922930 and NASA Heliophysics grant 80NSSC21K1557. VGM acknowledges support from the NASA DRIVE Science Center for Geospace Storms (CGS) under grant 80NSSC20K0601 and an LWS grant 80NSSC19K0080. AMPERE development, data acquisition, and science

processing at JHU/APL were supported by NSF awards ATM #0739864 and ATM #1420184. AMPERE data used in this paper are publicly available through the AMPERE web site (http://ampere.jhuapl.edu). MIDAS GPS-derived TEC data were used courtesy of the University of Bath, Claverton, Bath, UK. Input GPS data were obtained from the International GNSS Survey mirrors at http://garner.ucsd.edu/, ftp://geodesy.noaa.gov and ftp://data-out.unavco.org/. Solar and geomagnetic indices were obtained from https://omniweb.gsfc.nasa.gov/ and http://wdc.kugi.kyoto-u.ac.jp/. DMSP ion drift data were retrieved from http://cedar.openmadrigal.org/showExperiment?experiment_list=100118297 (UT Dallas files were used). DMSP processing code is available here: https://github.com/alexchartier/mix. Model output has been posted to https://zenodo.org/record/5218739#.YR10lNNKhb8

References

Anderson, B. J., K. Takahashi, and B. A. Toth (2000), Sensing global Birkeland currents

with Iridium engineering magnetometer data, Geophys. Res. Lett., 27(24), 4045–4048.

Anderson, B. J., K. Takahashi, T. Kamei, C. L. Waters, and B. A. Toth (2002), Birkeland current system key parameters derived from Iridium observations: Method and initial validation results, J. Geophys. Res., 107(A6), doi:10.1029/2001JA000080.

Anderson, B. J., H. Korth, C. L. Waters, D. L. Green, and P. Stauning (2008), Statistical Birkeland current distributions from magnetic field observations by the Iridium constellation, Ann. Geophys., 26, 671-687, doi:10.5194/angeo-26-671-2008.

Anderson, B. J., H. Korth, C. L. Waters, D. L. Green, V. G. Merkin, R. J. Barnes, and L. P. Dyrud (2014), Development of large-scale Birkeland currents determined from the Active Magnetosphere and Planetary Electrodynamics Response Experiment, Geophys. Res. Lett., 41(9), 3017–3025.

Anderson, B. J., Angappan, R., Barik, A., Vines, S. K., Stanley, S., Bernasconi, P. N., et al. (2021). Iridium communications satellite constellation data for study of Earth's magnetic field. *Geochemistry, Geophysics, Geosystems*, *22*, e2020GC009515. https://doi. org/10.1029/2020GC009515

Barrett, B., Raymond, J.W., & Goldfein, D.L. (2020), The Department of the Air Force Arctic Strategy. Retrieved from www.af.mil/Portals/1/documents/2020SAF/July/ArcticStrategy.pdf on 16 September 2020.

Bristow, W. A., Hampton, D. L., & Otto, A. (2016). High-spatial-resolution

velocity measurements derived using Local Divergence-Free Fitting of SuperDARN observations. *Journal of Geophysical Research: Space Physics*, *121*(2), 1349-1361.

Bust, G. S., Crowley, G., Garner, T. W., Gaussiran, T. L., Meggs, R. W., Mitchell, C. N., ... & Zapfe, B. (2007). Four-dimensional GPS imaging of space weather storms. *Space Weather*, *5*(2).

Chamberlin, P. C., Woods, T. N., & Eparvier, F. G. (2007). Flare irradiance spectral model (FISM): Daily component algorithms and results. *Space Weather*, *5*(7).

Chartier, A. T., Huba, J. D., & Mitchell, C. N. (2019). On the annual asymmetry of high-latitude sporadic F. *Space Weather*, *17*(11), 1618-1626.

Cousins, E. D., Matsuo, T., & Richmond, A. D. (2015). Mapping high-latitude ionospheric electrodynamics with SuperDARN and AMPERE. *Journal of Geophysical Research: Space Physics*, *120*(7), 5854-5870.

Dimant, Y. S., and M. M. Oppenheim (2011), Magnetosphere-ionosphere coupling through E region turbulence: 2. Anomalous conductivities and frictional heating, J. Geophys. Res., 116, A09304, doi:10.1029/2011JA016649.

Drob, D. P., Emmert, J. T., Meriwether, J. W., Makela, J. J., Doornbos, E., Conde, M., ... & Huba, J. D. (2015). An update to the Horizontal Wind Model (HWM): The quiet time thermosphere. *Earth and Space Science*, *2*(7), 301-319.

Fuller-Rowell, T. J., Rees, D., Quegan, S., Moffett, R. J., & Bailey, G. J. (1988). Simulations of the seasonal and universal time variations of the high-latitude thermosphere and ionosphere using a coupled, three-dimensional, model. In *Ionospheric Modelling* (pp. 189-217). Birkhäuser, Basel.

Gjerloev, J. W., Waters, C. L., & Barnes, R. J. (2018). Deriving global convection maps from SuperDARN measurements. *Journal of Geophysical Research: Space Physics*, 123, 2902– 2915. https://doi.org/10.1002/2017JA024543

Goodman, M. L. (1995), A three-dimensional, iterative mapping procedure for the implementation of an ionosphere-magnetosphere anisotropic Ohm's law boundary condition in global magnetohydrodynamic simulations, Ann. Geophys., 13, 843–853.

Hairston, M. R., & Heelis, R. A. (1993). *High-latitude electric field studies using DMSP data*. TEXAS UNIV AT DALLAS RICHARDSON CENTER FOR SPACE SCIENCES.

Hardy, D. A., Gussenhoven, M. S., & Holeman, E. (1985). A statistical model of auroral electron precipitation. *Journal of Geophysical Research: Space Physics*, *90*(A5), 4229-4248.

Hardy, D. A., Gussenhoven, M. S., & Brautigam, D. (1989). A statistical model of auroral ion precipitation. *Journal of Geophysical Research: Space Physics*, *94*(A1), 370-392.

Huba, J. D., G. Joyce, and J. A. Fedder. "Sami2 is Another Model of the Ionosphere (SAMI2): A new low-latitude ionosphere model." *Journal of Geophysical Research: Space Physics* 105, no. A10 (2000): 23035-23053.

Huba, J. D., G. Joyce, and J. Krall. "Three-dimensional equatorial spread F modeling." *Geophysical Research Letters*35, no. 10 (2008).

Lewis, H. R., and P. M. Bellan (1990), Physical constraints on the coefficients of Fourier expansions in cylindrical coordinates, *J. Math. Phys.*, **31**, 2592.1–2592.5, doi:10.1063/1.529009.

Maeda, K., Conductivity and drift in the ionosphere, J. Atmos. Terr. Phys., Vol.39, 1041-1053, 1977.

Matsuo, T., Kilcommons, L. M., Ruohoniemi, J. M., & Anderson, B. J. (2019). Assimilative Mapping of Geospace Observations (AMGeO): Data Science Tools for Collaborative Geospace Systems Science. *AGUFM*, *2019*, SM33A-01.

McGranaghan, R., Knipp, D. J., Matsuo, T., & Cousins, E. (2016). Optimal interpolation analysis of high-latitude ionospheric Hall and Pedersen conductivities: Application to assimilative ionospheric electrodynamics reconstruction. *Journal of Geophysical Research: Space Physics*, *121*(5), 4898-4923.

Merkin, V. G., and J. G. Lyon (2010), Effects of the low-latitude ionospheric boundary condition on the global magnetosphere, J. Geophys. Res., 115(A), A10202.

Merkin, V. G., Milikh, G., Papadopoulos, K., Lyon, J., Dimant, Y. S., Sharma, A. S., Goodrich, C., and Wiltberger, M. (2005), Effect of anomalous electron heating on the transpolar potential in the LFM global MHD model, *Geophys. Res. Lett.*, 32, L22101, doi:10.1029/2005GL023315.

Mitchell, C. N., & Spencer, P. S. (2003). A three-dimensional time-dependent algorithm for ionospheric imaging using GPS. Annals of Geophysics, 46(4), 687-696.

Picone, J. M., Hedin, A. E., Drob, D. P., & Aikin, A. C. (2002). NRLMSISE-00 empirical model of the atmosphere: Statistical comparisons and scientific issues. *Journal of Geophysical Research: Space Physics*, *107*(A12), SIA-15.

Quegan, S., Bailey, G. J., Moffett, R. J., Heelis, R. A., Fuller-Rowell, T. J., Rees, D., & Spiro, R. W. (1982). A theoretical study of the distribution of ionization in the high-latitude ionosphere and the plasmasphere: First results on the mid-latitude trough and the light-ion trough. *Journal of Atmospheric and Terrestrial Physics*, *44*(7), 619-640.

Ramirez, U., Wang, N., Chartier, A. T., & Datta-Barua, S. (2019). SuperDARN Evidence for Convection-Driven Lagrangian Coherent Structures in the Polar Ionosphere. *Journal of Geophysical Research: Space Physics*, *124*(5), 3573-3588.

Richards, P. G., Fennelly, J. A., & Torr, D. G. (1994). EUVAC: A solar EUV flux model for aeronomic calculations. *Journal of Geophysical Research: Space*

Physics, *99*(A5), 8981-8992.

Richmond, A. D. (1995), Ionospheric electrodynamics using magnetic apex coordinates, J. Geomagn. Geoelectr., 47, 191–212.

Robinson, R. M., & Vondrak, R. R. (1984). Measurements of E region ionization and conductivity produced by solar illumination at high latitudes. *Journal of Geophysical Research: Space Physics*, *89*(A6), 3951-3956.

Robinson, R. M., Vondrak, R. R., Miller, K., Dabbs, T., & Hardy, D. (1987). On calculating ionospheric conductances from the flux and energy of precipitating electrons. *Journal of Geophysical Research: Space Physics*, *92*(A3), 2565-2569.

Robinson, R. M., Kaeppler, S. R., Zanetti, L., Anderson, B., Vines, S. K., Korth, H., & Fitzmaurice, A. (2020). Statistical relations between auroral electrical conductances and field-aligned currents at high latitudes. *Journal of Geophysical Research: Space Physics*, *125*(7), e2020JA028008.

Roble, R. G., Ridley, E. C., Richmond, A. D., & Dickinson, R. E. (1988). A coupled thermosphere/ionosphere general circulation model. *Geophysical Research Letters*, *15*(12), 1325-1328.

Roble, R. G., & Ridley, E. C. (1994). A thermosphere-ionosphere-mesosphere-electrodynamics general circulation model (TIME-GCM): Equinox solar cycle minimum simulations (30–500 km). *Geophysical Research Letters*, *21*(6), 417-420.

Ruohoniemi, J. M., and Baker, K. B. (1998), Large-scale imaging of high-latitude convection with Super Dual Auroral Radar Network HF radar observations, *J. Geophys. Res.*, 103(A9), 20797– 20811, doi:10.1029/98JA01288.

Sorathia, K. A., Merkin, V. G., Panov, E. V., Zhang, B., Lyon, J. G., & Garretson, J., et al. (2020). Ballooning-interchange instability in the near-Earth plasma sheet and auroral beads: Global magnetospheric modeling at the limit of the MHD approximation. Geophysical Research Letters, 47, e2020GL088227. https://doi.org/10.1029/2020GL088227

Spencer, P. S. J.; Mitchell, C. N. (2007), Imaging of fast moving electron-density structures in the polar cap. Annals of Geophysics, [S.l.], v. 50, n. 3, dec. 2007. ISSN 2037-416X.

Wang, N., Datta-Barua, S., Chartier, A. T., Ramirez, U., & Mitchell, C. N. (2018). Horseshoes in the High-Latitude Ionosphere. *Journal of Geophysical Research: Space Physics*, *123*(7), 5831-5849.

Waters, C. L., B. J. Anderson, and K. Liou (2001), Estimation of global field aligned currents using the Iridium® system magnetometer data, Geophys. Res. Lett., 28, 2165-2168, doi:10.1029/2000GL012725.

Waters, C.L., B. J. Anderson, D. L. Green, H. Korth, R. J. Barnes, H. Vanhamäki (2020), Science Data Products for AMPERE, *in Ionospheric Multi-Spacecraft Analysis Tools*, *ISSI Scientific Report Series*, **17**, edited by M. Dunlop

and H. Lühr, Springer, pp. 141 – 165, Cham, Switzerland, doi:10.1007/978-3-030-26732-2_7.

Weimer, D. R. (2005). Predicting surface geomagnetic variations using ionospheric electrodynamic models. Journal of Geophysical Research, 110, A12307. https://doi.org/10.1029/2005JA011270

Wiltberger, M., et al. (2017), Effects of electrojet turbulence on a magnetosphere-ionosphere simulation of a geomagnetic storm, *J. Geophys. Res. Space Physics*, 122, 5008– 5027, doi:10.1002/2016JA023700.

Wolf, R. A. (1983), The Quasi-Static (Slow-Flow) Region of the magnetosphere, in Solar-Terrestrial Physics, edited by R. L. Carovillano and J. M. Forbes, pp. 303–368, D. Reidel, Dordrecht, Netherlands.

Zhang, B., Lotko, W., Brambles, O., Wiltberger, M. and Lyon, J. (2015), Electron precipitation models in global magnetosphere simulations. *J. Geophys. Res. Space Physics*, 120: 1035– 1056. doi: 10.1002/2014JA020615.